

THE MEASUREMENT OF THE f_s/f_d RATIO FROM HADRONIC MODES IN THE LHCb EXPERIMENT*

PIOTR MORAWSKI

for the LHCb Collaboration

The Henryk Niewodniczański Institute of Nuclear Physics
Polish Academy of Sciences
Radzikowskiego 152, 31-342 Kraków, Poland

(Received May 8, 2012)

In this paper, the measurement of the fragmentation factor ratio f_s/f_d in the LHCb experiment using hadronic decay modes is presented. The relative yields of the three channels $B^0 \rightarrow D^- \pi^+$, $B^0 \rightarrow D^- K^+$, $B_s^0 \rightarrow D_s^- \pi^+$ selected from 35 pb^{-1} of data collected in 2010 are used for the analysis. The fragmentation fraction ratio is determined to be $f_s/f_d = 0.245 \pm 0.017^{\text{stat}} \pm 0.018^{\text{syst}} \pm 0.018^{\text{theor}}$.

DOI:10.5506/APhysPolB.43.1561

PACS numbers: 11.30.Er, 12.15.Hn, 13.25.Hw

1. Introduction

The fragmentation fractions f_d , f_s , f_u , f_Λ determine the probability that the quark hadronizes into the specific B_q meson (where $q = d, s, u$) or Λ_b baryon. The measurement of f_s/f_d is particularly important for measurements of B_s^0 branching fractions, as few normalization modes have precisely measured branching fractions. One of the prime examples is the measurement of the $\mathcal{B}(B_s^0 \rightarrow \mu\mu)$ branching fraction, where the uncertainty of f_s/f_d measurement is the main contribution to the systematic uncertainty [1].

Three charm hadronic decays¹ are employed for this analysis: $B^0 \rightarrow D^- \pi^+$, $B^0 \rightarrow D^- K^+$ and $B_s^0 \rightarrow D_s^- \pi^+$. The $B_s^0 \rightarrow D_s^- \pi^+$ and $B^0 \rightarrow D^- K^+$ decay amplitudes are described by colour-allowed tree-diagrams only, thus they are theoretically well predicted. The $B^0 \rightarrow D^- \pi^+$ amplitude is less

* Presented at the Cracow Epiphany Conference on Present and Future of B Physics, Cracow, Poland, January 9–11, 2012.

¹ In the following, the decays stand for charge conjugated processes as well.

clean since it receives a W exchange diagram contribution whose size must be estimated relative to the three diagrams. One can extract the f_s/f_d ratio in two different ways.

The first approach uses the $B_s^0 \rightarrow D_s^- \pi^+$ and $B^0 \rightarrow D^- K^+$ channels. The advantage of this approach is that signals can be extracted in a theoretically clean way for both channels. On the other hand, the statistic for the $B^0 \rightarrow D^- K^+$ decays is reduced, since it is a Cabibbo suppressed channel. The ratio of the branching fractions can be calculated as follows [2]

$$\frac{\mathcal{B}(B_s^0 \rightarrow D_s^- \pi^+)}{\mathcal{B}(B^0 \rightarrow D^- K^+)} = \frac{\tau_{B_s^0}}{\tau_{B^0}} \left| \frac{V_{ud}}{V_{us}} \right|^2 \left(\frac{f_\pi}{f_K} \right)^2 \left[\frac{F_0^{(s)}(m_\pi^2)}{F_0^{(d)}(m_K^2)} \right]^2 \left| \frac{a_1(D_s^- \pi^+)}{a_1(D^- K^+)} \right|^2, \quad (1)$$

where τ_B is the lifetime of the B meson, V_{ud} and V_{us} are the relevant CKM elements, $f_{\pi,K}$ is the decay constant for the pion or kaon and $F_0(q^2)$ is the value of the form factor at the 4-momentum transfer q . The $a_1(D_q h)$ factors take into account the deviation from the factorization assumed. On the other hand, the yields of the two channels are related as follows

$$\frac{N_{D_s \pi}}{N_{DK}} = \frac{f_s \epsilon_{D_s \pi}}{f_d \epsilon_{DK}} \frac{\mathcal{B}(B_s^0 \rightarrow D_s^- \pi^+)}{\mathcal{B}(B^0 \rightarrow D^- K^+)}, \quad (2)$$

where ϵ is the total detector efficiency which includes various effects arising from trigger, offline selection and reconstruction efficiencies. These efficiencies are being calculated separately for each mode using samples of simulated signal events. Taking the values of various factors from [2,3], the f_s/f_d ratio is given by the following expression

$$\frac{f_s}{f_d} = 0.0743 \times \frac{\tau_{B^0}}{\tau_{B_s^0}} \times \left[\frac{1}{\mathcal{N}_a \mathcal{N}_F} \frac{\epsilon_{DK}}{\epsilon_{D_s \pi}} \frac{N_{D_s \pi}}{N_{DK}} \right], \quad (3)$$

with

$$\begin{aligned} \mathcal{N}_a &\equiv \left| \frac{a_1(D_s^- \pi^+)}{a_1(D^- K^+)} \right|^2 = 1.00 \pm 0.02 [4], \\ \mathcal{N}_F &\equiv \left[\frac{F_0^{(s)}(m_\pi^2)}{F_0^{(d)}(m_K^2)} \right]^2 = 1.24 \pm 0.08 [5]. \end{aligned} \quad (4)$$

The second method employs $B^0 \rightarrow D^- \pi^+$ and $B_s^0 \rightarrow D_s^- \pi^+$ decay channels. This method profits from the high branching fraction of the $B^0 \rightarrow D^- \pi^+$ that can significantly reduce the statistical uncertainties. In analogy to the former method f_s/f_d can be expressed as [4]

$$\frac{f_s}{f_d} = 0.982 \times \frac{\tau_{B^0}}{\tau_{B_s^0}} \times \left[\frac{1}{\mathcal{N}_a \mathcal{N}_F \mathcal{N}_E} \frac{\epsilon_{D\pi}}{\epsilon_{D_s \pi}} \frac{N_{D_s \pi}}{N_{D\pi}} \right], \quad (5)$$

where an additional \mathcal{N}_E factor is the contribution arising from the exchange diagrams. The value of this term has been calculated to be $\mathcal{N}_E = 0.966 \pm 0.075$.

The yields are extracted by fitting the three invariant mass distributions independently for each signal channel by means of unbinned maximum likelihood method.

2. The LHCb detector and data sample

The LHCb detector [6] is a single arm spectrometer designed to study the decays of B mesons at the LHC. The sensitive area of the detector covers the angles between 15 mrad and 300 mrad. This corresponds to the pseudorapidity range of $1.8 < \eta < 4.9$. The trigger system consists of the hardware trigger L0 and the High Level Trigger (HLT) implemented in the software. The L0 trigger selects events with high p_T tracks to reduce the rate of bunch crossings from about 11 MHz down to 1 MHz. The partial event reconstruction takes place in the first step of software trigger (HLT1) while the more complete reconstruction is performed in the second step (HLT2). The software trigger reduces the event rate further down to about 2 kHz.

The two subsystems of the whole LHCb detector are crucial for this analysis. The precise vertex detector (VELO) is able to effectively distinguish between the primary and secondary vertices. For high multiplicity primary vertices the resolution is $12 \mu\text{m}$ in the direction transverse to the beam axis and $50 \mu\text{m}$ along the beam. The two Cherenkov radiation detectors provide a good distinction between kaons and pions in the range of 2–100 GeV.

The data sample used for this analysis consists of 35 pb^{-1} of data collected by the LHCb experiment in 2010 at the centre-of-mass energy of 7 TeV.

3. Selection procedure

The selection of $B^0 \rightarrow D^- \pi^+$, $B^0 \rightarrow D^- K^+$, and $B_s^0 \rightarrow D_s^- \pi^+$ modes is done in such a way that it minimizes the efficiency difference between the channels. Since all the modes have a similar decay topology, the selection is designed to use the topological information only. This is ensured in both the trigger and off-line selections.

3.1. Trigger

The hardware trigger (L0) requires one cluster with a transverse energy deposition greater than 3.6 GeV in the hadronic calorimeter. HLT1 demands one high p_T track well displaced from the primary interaction point. In the HLT2 step the topological trigger [7] reconstructs a 2, 3 or 4-prong secondary vertex with a high sum of p_T of the outgoing tracks. The vertex has to be significantly separated from the primary vertex.

The difference in efficiencies for signal modes observed in L0 arise mainly due to higher K efficiency in this level of trigger, thus modes with bachelor (the light hadronic B child) kaon are $\approx 2\%$ more efficient. The discrepancies occur also in HLT and the main reason for that is the difference in the D and D_s^+ lifetimes. It causes the reconstructed track (in HLT1) and vertex (in HLT2) to be better separated for B^0 than B_s^0 . The relative correction factor of 1.081 ± 0.024 for B_s^0 with respect to B^0 has been introduced to compensate for this effect.

3.2. Offline selection

To optimize the selection while taking into account the correlation between various variables, a multivariate analysis (MVA) technique is used [8]. The TMVA software package [9] containing a number of MVA methods is employed. The “gradient” decision tree method was found to have the best performance (see Fig. 1) and to be the least sensitive to overtraining.

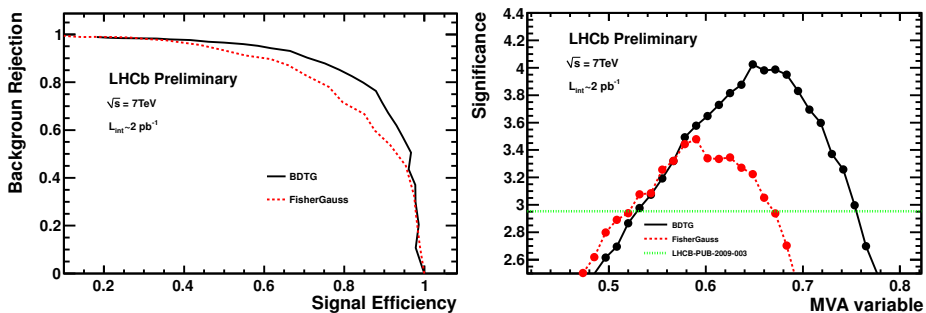


Fig. 1. Comparison of MVA methods. Receiver Operating Characteristics (ROC) curve (left), significance (right). BDTG (solid/black), FischerGauss (dotted/red), rectangular cuts (horizontal grey/green)

A sample of simulated $B^0 \rightarrow D^- \pi^+$ signal events was used for training. The comparison of distributions of the input variables for the real data and the simulated sample shows good agreement which justifies the use of simulated data. The distributions for background are extracted from the B mass sidebands for the fraction of the total sample corresponding to 2pb^{-1} . The selection is optimized to achieve the best significance for the Cabibbo suppressed mode. Variables related to $D(D_s^+)$ lifetime are excluded to minimize the difference between B^0 and B_s^0 modes. The selection efficiency for the events accepted by trigger is $\approx 75\%$ for the three modes.

Finally, particle identification (PID) is imposed on the bachelor hadron to distinguish between the modes. The log-likelihood difference of the kaon and pion hypothesis is used. We demand $\text{DLL}_{K\pi} < 0$ for the bachelor

pion and $DLL_{K\pi} > 5$ for the bachelor kaon. B^0 and B_s^0 modes are in addition distinguished by the different mass window to select the D^0 and D_s^+ candidates, respectively.

3.3. Correction factors

Besides the differences in efficiencies that arise due to trigger and particle identification cuts used for the specific signal modes, a tracking efficiency difference for kaons and pions has a significant impact on the final measurement. The ratio of signal yields have to be corrected based on these specific correction factors. The precise numbers are presented in Table I.

TABLE I

Correction factors for the f_s/f_d measurements.

| Efficiency ratio | $\frac{\epsilon_{DK}}{\epsilon_{D_s\pi}}$ | $\frac{\epsilon_{D\pi}}{\epsilon_{D_s\pi}}$ |
|---------------------------------------|---|---|
| K^\mp/π^\pm tracking eff. | 1.014 ± 0.004 | 1.039 ± 0.003 |
| PID cuts | 0.959 ± 0.006 | 1.135 ± 0.005 |
| Bach. $K^\mp P < 100 \text{ GeV}/c^2$ | 0.993 ± 0.001 | n/a |
| Trigger eff. | 0.925 ± 0.020 | 0.925 ± 0.020 |
| Total | 0.893 ± 0.020 | 1.091 ± 0.025 |

4. Fitting model

The extraction of the event yields requires a precise description of signal and background components that are visible in the B mass distribution.

4.1. Signal model

To properly describe the signal mass peak, various detector effects have to be taken into account. Multiple scattering and reconstruction distortion cause the symmetric, Gaussian like, tail on both sides of the peak. The radiative tail is present due to final state radiation for B and D meson decays. Such low energy radiative photons are not taken into account during the event reconstruction. In effect, an asymmetric tail towards the lower invariant mass region is observed. The shape of the signal mass peak has been determined using a sample of simulated events. The combination of two Crystal Ball (CB) [10, 11] functions has been chosen. The parameters describing the CB tails are determined on the basis of simulation and then fixed. We assume the same mean value for both CB functions. The other parameters are left free in the fitter.

4.2. Background model

There are three categories of background to be considered. The source of the first category is combinatorics. It consists of random kaon or pion associated to a real D . The shape can be determined from data using the events with incorrect combinations of the D and the bachelor hadron, D^+h^+ or D^-h^- . Its non-peaking character can be described using an exponential shape. Specifically in the case of $B^0 \rightarrow D^-K^+$, the combinatoric background was parametrized by a straight line.

The second type of background comes from partially reconstructed B meson decays. The most important are channels with missing π^0 : $B^0 \rightarrow D^{*-}\pi^+$ and $B^0 \rightarrow D^-\rho^+$. Under the $B^0 \rightarrow D^-K^+$ mass hypothesis those two background components are present with misidentified bachelor π^+ . Their shapes are extracted from the simulation and fixed allowing the normalization to float during the fitting procedure. These shapes are shown in Fig. 2.

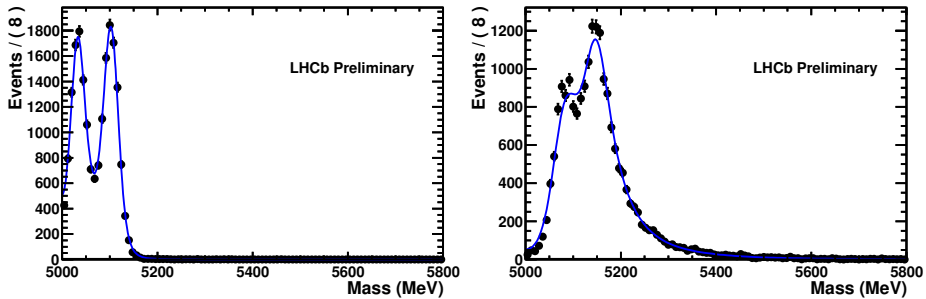


Fig. 2. The shape of partially reconstructed physical background $B^0 \rightarrow D^{*-}\pi^+$ under correct mass hypothesis (left) and with bachelor kaon mass hypothesis (right)

The last type of background is the reflection from real decays with wrong mass hypothesis assigned due to misidentification of decay products. Particle identification cuts are introduced on the bachelor hadron and D children to improve the precision of yield extraction. The contamination from $B_s^0 \rightarrow D_s^- \pi^+$ in the $B^0 \rightarrow D^- \pi^+$ and $B^0 \rightarrow D^- K^+$ samples is estimated to be negligible. The contamination from Λ_b is expected to be at the level of 1% for $B^0 \rightarrow D^- \pi^+$ and 2% for $B^0 \rightarrow D^- K^+$. We do not impose any correction for the reflection from Λ_b and assign a 2% systematic uncertainty. In the case of $B_s^0 \rightarrow D_s^- \pi^+$ decay the Λ_b background is no longer negligible. The expected shape of Λ_b contamination is extracted from the simulated events and included in the fitting model.

To model the reflections due to misidentification of the bachelor particle we use a method of reweighing already fitted shapes to get the shapes under new mass hypothesis. We explain the method for the $B^0 \rightarrow D^- \pi^+$ mode under bachelor kaon mass hypothesis. The number of signal events and

misidentified events is roughly the same in that sample since the relatively small misidentification probability is compensated by the large branching ratio of $B^0 \rightarrow D^- \pi^+$. Firstly, a sample of clean $B^0 \rightarrow D^- \pi^+$ events is prepared with the $\text{DLL}_{K\pi} < 0$ cut and bachelor kaon hypothesis. Since the $\text{DLL}_{K\pi}$ cut efficiency is momentum dependent, the distribution must be corrected for the distortions introduced by the particle identification cut. As a result, the distribution of mass under the incorrect particle hypothesis without any momentum biases can be obtained. As the sample of $B^0 \rightarrow D^- K^+$ is selected using $\text{DLL}_{K\pi} > 5$ the performance of this cut must be evaluated. It is done using D^* decays. The result can be seen in Fig. 3. The final step is to reweigh the distribution according to the $\text{DLL}_{K\pi}$ cut efficiency. The mass distribution before and after the reweighing procedure is shown in Fig. 3.

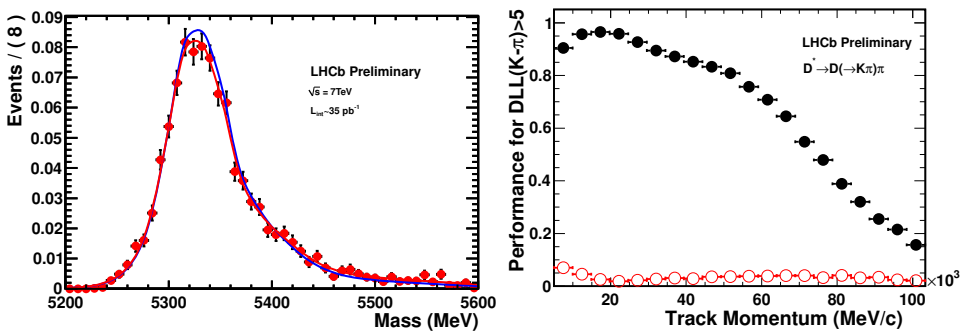


Fig. 3. Left: Mass shape of $B^0 \rightarrow D^- \pi^+$ events with the bachelor misidentified as a kaon, for a PID cut of $\text{DLL}_{K\pi} > 5$, before (black/blue) and after (grey/red) reweighing. Right: Probability, as a function of momentum, to correctly identify a kaon (full black circles) and to wrongly identify a pion as a kaon (open/red circles), for a PID cut of $\text{DLL}_{K\pi} > 5$.

4.3. Fitting model validation

The fitting components are merged into three distinct fitting models, one for each signal channel. The stability and accuracy of these models have been checked by series of MC pseudo-experiments. In this way, we have shown that the fitting results are unbiased and the uncertainties are estimated correctly.

Various additional cross checks are performed. The values of parameters that are fixed in the fitter are varied by a few percent and a systematic is assigned according to the obtained result. Additionally, the number of events from misidentified backgrounds is estimated from the knowledge of signal yield under the proper mass hypothesis and misidentification probability. In all cases, the number of events is compatible with the estimation.

Finally, the cocktail sample is produced by fully simulated events containing a mixture of $B^0 \rightarrow D^- \pi^+$, $B^0 \rightarrow D^- K^+$, $B^0 \rightarrow D^- \rho^+$, $B^0 \rightarrow D^{*-} \pi^+$, $A_b \rightarrow \Lambda_c \pi^-$ and inclusive $b\bar{b}$ events for the combinatoric contribution. The fitter is able to accurately reproduce the initial composition.

5. Fitting results

The results of the fit to the $B^0 \rightarrow D^- \pi^+$ and $B^0 \rightarrow D^- K^+$ are shown in Fig. 4. The extracted number of events for $B^0 \rightarrow D^- \pi^+$ and $B^0 \rightarrow D^- K^+$ are 4103 ± 75 and 252 ± 21 , respectively. The number of misidentified $B^0 \rightarrow D^- \pi^+$ events under bachelor kaon mass hypothesis is 131 ± 19 . It is consistent with 145 ± 5 events estimated using the knowledge of the misidentification efficiency extracted from the D^* sample.

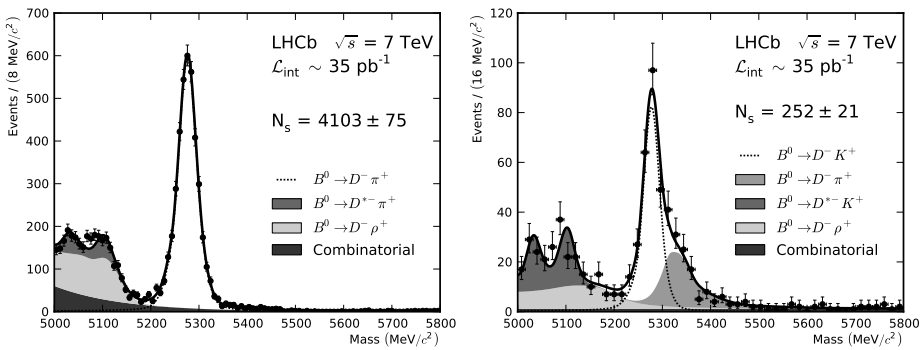
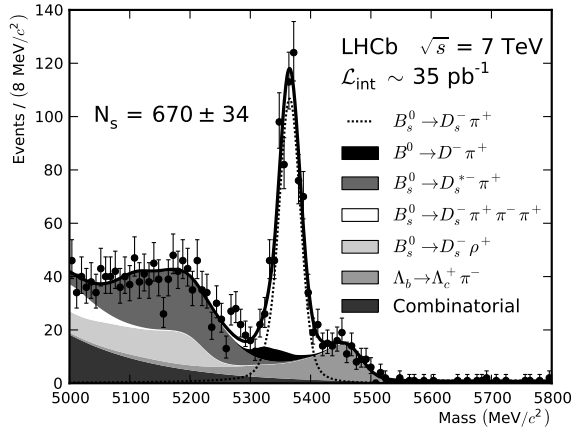


Fig. 4. Results of the fit to $B^0 \rightarrow D^- \pi^+$ (left) and $B^0 \rightarrow D^- K^+$ (right) candidates.

The $B_s^0 \rightarrow D_s^- \pi^+$ fitting procedure differs in several aspects. The widths of CB functions in the B_s^0 fitter were fixed to 83% and 91% of the values extracted from the $B^0 \rightarrow D^- \pi^+$ fitter. The rescaling is based on the comparison between the $B^0 \rightarrow D^- \pi^+$ and $B_s^0 \rightarrow D_s^- \pi^+$ simulated samples. The shape of misidentified $B^0 \rightarrow D^- \pi^+$ peak and its yield is fixed due to overlap with the $B_s^0 \rightarrow D_s^- \pi^+$ signal having a similar shape. We fix the ratio of partially reconstructed backgrounds $B_s^0 \rightarrow D_s^- \rho^+$ and $B_s^0 \rightarrow D_s^{*-} \pi^+$ to further increase the fitter stability. The ratio is taken from the results of the $B^0 \rightarrow D^- \pi^+$ fit and constrained with the Gaussian probability to account for differences between B^0 and B_s^0 systems. A Gaussian width of 20% of the mean value of the ratio is chosen. The number of fitted $B_s^0 \rightarrow D_s^- \pi^+$ events is 670 ± 34 and is shown in Fig. 5.


 Fig. 5. Results of the fit to $B_s^0 \rightarrow D_s^- \pi^+$ candidates.

6. Result

From equations 3 and 5 and the fitted yields of $B^0 \rightarrow D^- \pi^+$, $B^0 \rightarrow D^- K^+$ and $B_s^0 \rightarrow D_s^- \pi^+$ decays, the f_s/f_d ratio can be extracted in two different ways: comparing $B^0 \rightarrow D^- K^+$ to $B_s^0 \rightarrow D_s^- \pi^+$ or $B^0 \rightarrow D^- \pi^+$ to $B_s^0 \rightarrow D_s^- \pi^+$. For the calculations of f_s/f_d using the first method, the current world average is assumed for B_s^0 to B^0 lifetime ratio, $\tau_{B_s^0}/\tau_{B^0} = 0.973 \pm 0.015$. The combined factor accounting for the non-factorizable corrections and form factors is taken from [2]: $\mathcal{N}_a \mathcal{N}_F = 1.24 \pm 0.08$. Using $\mathcal{B}(D^+ \rightarrow K^- \pi^+ \pi^+) = (9.14 \pm 0.20)\%$ [12] and $\mathcal{B}(D_s^+ \rightarrow K^- K^+ \pi^+) = (5.50 \pm 0.27)\%$ the f_s/f_d is found to be

$$\frac{f_s}{f_d} = 0.242 \pm 0.024^{\text{stat}} \pm 0.018^{\text{syst}} \pm 0.016^{\text{theor}}. \quad (6)$$

Using the second method an additional uncertainty from the W -exchange diagrams [4], $\mathcal{N}_E = 0.966 \pm 0.075$ needs to be introduced:

$$\frac{f_s}{f_d} = 0.249 \pm 0.013^{\text{stat}} \pm 0.020^{\text{syst}} \pm 0.025^{\text{theor}}. \quad (7)$$

The two measurements are consistent.

The systematic uncertainties for these two measurements are listed in Table II. The systematic uncertainty which originates from the PID calibration has less impact on the first measurement since the final states for $B^0 \rightarrow D^- K^+$ and $B_s^0 \rightarrow D_s^- \pi^+$ are the same (*i.e.* $K^- K^+ \pi^+$).

These two values for f_s/f_d can be combined into one. All the correlation between the uncertainties needs to be taken into account. The averaged value of f_s/f_d is

$$\frac{f_s}{f_d} = 0.245 \pm 0.017^{\text{stat}} \pm 0.018^{\text{syst}} \pm 0.018^{\text{theor}}. \quad (8)$$

TABLE II

Systematic uncertainties for the f_s/f_d measurements.

| Source | For $D_s^- \pi^+ / D^- K^+$ | For $D_s^- \pi^+ / D^- \pi^+$ |
|--|-----------------------------|-------------------------------|
| PID calibration | 1.5% | 2.5% |
| B^0 fit model | 2% | 2% |
| B_s^0 fit model | 2% | 2% |
| L0 trigger efficiency | 2% | 2% |
| $\mathcal{B}(D_s^\pm \rightarrow KK\pi)$ | 4.9% | 4.9% |
| $\mathcal{B}(D^\pm \rightarrow K\pi\pi)$ | 2.2% | 2.2% |
| $\frac{\tau_{B^0}}{\tau_{B^0}}$ | 1.5% | 1.5% |
| Correction factors | 2.2% | 2.2% |
| Total | 7.0% | 7.4% |

7. Summary

On the basis of 35 pb^{-1} of data collected in 2010 by the LHCb experiment at 7 TeV centre-of-mass energy the measurement of f_s/f_d ratio has been conducted using two approaches: by comparing $B^0 \rightarrow D^- K^+$ to $B_s^0 \rightarrow D_s^- \pi^+$ and $B^0 \rightarrow D^- \pi^+$ to $B_s^0 \rightarrow D_s^- \pi^+$. The combined value of $\frac{f_s}{f_d}$ has been calculated to be $0.245 \pm 0.017^{\text{stat}} \pm 0.018^{\text{syst}} \pm 0.018^{\text{theor}}$.

REFERENCES

- [1] R. Aaij *et al.* [LHCb Collaboration], *Phys. Lett.* **B699**, 330 (2011) [arXiv:1103.2465v2 [hep-ex]].
- [2] R. Fleischer, N. Serra, N. Tuning, *Phys. Rev.* **D82**, 034038 (2010) [arXiv:1004.3982v3 [hep-ph]].
- [3] J.L. Rosner, S. Stone, arXiv:1002.1655v2 [hep-ex].
- [4] R. Fleischer, N. Serra, N. Tuning, *Phys. Rev.* **D83**, 014017 (2011) [arXiv:1012.2784v2 [hep-ph]].
- [5] P. Blasi, P. Colangelo, G. Nardulli, N. Paver, *Phys. Rev.* **D49**, 238 (1994) [arXiv:hep-ph/9307290v1].

- [6] A.A. Alves Jr. *et al.*, *JINST* **3**, S08005 (2008).
- [7] M. Williams *et al.*, The HLT2 Topological Lines, Tech. Rep. LHCb-PUB-2011-002, CERN, Geneva, Jan 2011.
- [8] S. Easo, Selection of $B_s^0 \rightarrow D_s^- K^+$ and $B_s^0 \rightarrow D_s^- \pi^+$ Decay Modes in LHCb Using Multivariate Methods, LHCb-PUB-2010-009, 2010.
- [9] A. Hoecker *et al.*, *PoS ACAT*, 040 (2007) [[arXiv:physics/0703039v5](https://arxiv.org/abs/physics/0703039v5)] [[physics.data-an](https://arxiv.org/abs/physics.data-an)].
- [10] J. Gaiser, Charmonium Spectroscopy from Radiative Decays of the J/ψ and ψ' , Ph.D. Thesis, Appendix F, SLAC-R-255, 1982.
- [11] T. Skwarnicki, A Study of the Radiative Cascade Transitions Between the Υ and Υ' resonances, Ph.D. Thesis, Appendix E, DESY F31-86-02, 1986.
- [12] S. Dobbs *et al.* [CLEO Collaboration], *Phys. Rev.* **D76**, 112001 (2007) [[arXiv:0709.3783v2](https://arxiv.org/abs/hep-ex/0709.3783v2)] [[hep-ex](https://arxiv.org/abs/hep-ex)].